SCIENCE CHINA
Physics, Mechanics & Astronomy

• Article •

July 2024 Vol. 67 No. 7: 272011
https://doi.org/10.1007/s11433-023-2342-4

Principal components of nuclear mass models

Xin-Hui Wu[1,2*], and Pengwei Zhao[2*]

[1] *Department of Physics, Fuzhou University, Fuzhou 350108, China;*
[2] *State Key Laboratory of Nuclear Physics and Technology, School of Physics, Peking University, Beijing 100871, China*

Received December 15, 2023; accepted February 5, 2024; published online May 20, 2024

Principal component analysis (PCA) is employed to extract the principal components (PCs) present in nuclear mass models for the first time. The effects from different nuclear mass models are reintegrated and reorganized in the extracted PCs. These PCs are recombined to build new mass models, which achieve better accuracy than the original theoretical mass models. This comparison indicates that using the PCA approach, the effects contained in different mass models can be collaborated to improve nuclear mass predictions.

nuclear mass, principal component analysis, nuclear models, statistical methods

PACS number(s): 21.10.Dr, 21.45.-v, 29.85.-c

Citation: X.-H. Wu, and P. Zhao, Principal components of nuclear mass models, Sci. China-Phys. Mech. Astron. **67**, 272011 (2024), https://doi.org/10.1007/s11433-023-2342-4

1 Introduction

Nuclear masses are extremely important in nuclear physics, as they reflect many underlying physical effects of nuclear structure information [1]. Nuclear masses are also crucial for astrophysics, as they are needed to extract the reaction energies used to calculate all nuclear reaction rates involved in stellar evolutions [2-6]. With the development of modern accelerator facilities, approximately 2500 nuclear masses have been measured thus far [7]. Nevertheless, a large unknown region in the nuclear landscape cannot be accessed experimentally, at least in the foreseeable future.

Theoretical prediction of nuclear mass has been a massive challenge in nuclear physics owing to the difficulties in understanding the nuclear interactions and the quantum many-body systems. Theoretical prediction of nuclear mass can be traced back to the macroscopic Weizsäcker mass formula based on the liquid drop model (LDM) [8], which includes the bulk properties of nuclei quite well but lacks other effects. Efforts have been made in pursuing extensions of the LDM to include more effects, which are known as macroscopic-microscopic models [9-12]. Microscopic mass models based on the nonrelativistic and relativistic density functionals have also been developed [13-25]. Additionally, the local mass relations such as the Garvey-Kelson relations [26, 27], the isobaric multiplet mass equation [28], and the residual proton-neutron interactions [29] are used to predict the masses of nuclei near the known region.

To precisely describe nuclear masses, one should, in principle, properly address all the underlying effects of nuclear quantum many-body systems, e.g., bulk effects, deformation effects, shell effects, odd-even effects, and even some unknown effects. Various models include these effects to different degrees. Some models properly consider only some of these effects, while other models properly consider only some other effects. With so many mass models available,

*Corresponding authors (Xin-Hui Wu, email: wuxinhui@fzu.edu.cn; Pengwei Zhao, email: pwzhao@pku.edu.cn)

one may ask, can we extract the major patterns considered in these models? Moreover, can we refine the nuclear mass predictions by recombining the extracted patterns?

Recently, machine learning approaches have attracted considerable attention in physics and nuclear physics [30-37] and have been successfully and widely employed in refining the predictions of nuclear masses, e.g., the kernel ridge regression (KRR) [38-43], the radial basis function (RBF) [44-47], the neural network (NN) [48-52], the Gaussian process regression [53, 54], the Levenberg-Marquardt neural network [55], the light gradient boosting machine [56], the Bayesian probability classifier [57], and the probably approximately correct learning [58]. These successes encourage us to employ statistical techniques to analyze the major effects contained in nuclear mass models. Principal component analysis (PCA) is a popular statistical technique for feature selection and dimensionality reduction [59, 60]. Thus, PCA has been applied to the studies of nuclear physics, e.g., to remove spurious events in the measurement of $2\nu\beta\beta$ decay [61], to evaluate the uncertainty in the neutrino-nucleus scattering cross section [62], to study event-by-event fluctuations in relativistic heavy-ion collisions [63], to reduce the dimensions of many-body problems [64], to optimize the functional derivatives of nuclear energy density functionals [65], to analyze the correlation of parameters in nuclear energy density functionals [66], to quantify the uncertainty of empirical shell-model interactions [67], to learn about the number of effective parameters in the LDM and the Skyrme functional [68], and to define empirical basis functions capturing the variation in the output of Hartree-Fock-Bogoliubov calculations [69].

Herein, for the first time, the PCA approach is employed to extract the principal components (PCs) contained in several widely used nuclear mass models. The commonalities and differences across different mass models are analyzed with the help of these PCs. These PCs are then recombined to build new mass models. This differs from the existing work of applying PCA to nuclear mass studies [68], where PCA is employed to learn about the number of effective parameters in the LDM and the Skyrme functional.

2 Theoretical framework

PCA is a technique used for identifying a set of PCs that capture the maximum features in data [59, 60]. This analysis is achieved by transforming the origin variables into a new set of variables, the PCs, which are uncorrelated and which are ordered so that the first few variables retain most of the features present in all of the original variables.

When applying PCA to nuclear mass models, the original variables are the mass predictions of different nuclear models, i.e., original nuclear mass tables. These original variables are correlated. They share many effects in common. After performing PCA, they are transformed into a new set of "principal mass models", which are uncorrelated and arranged in the order of importance in representing the relevant features extracted from the original mass models.

The PCA application to nuclear mass models includes the following steps.

- First, pick up N mass models that will be analyzed, e.g., model-1, model-2, $\cdots$, model-N.
- Second, vectorize the mass predictions of these mass models into high-dimension vectors with m components (corresponding to m nuclei in the nuclear chart), i.e., $\boldsymbol{M}_1$, $\boldsymbol{M}_2$, $\cdots$, $\boldsymbol{M}_N$, namely, the "original mass-model vectors".
- Third, construct the covariance matrix of these N original mass-model vectors, $\boldsymbol{C} = \boldsymbol{X}^\top \boldsymbol{X}$, where $\boldsymbol{X}$ is a $N \times m$ matrix defined as $\boldsymbol{X} = (\boldsymbol{M}_1, \boldsymbol{M}_2, \cdots, \boldsymbol{M}_N)^\top$. Because the covariance matrix is constructed from N original mass-model vectors, its rank is N.
- Fourth, diagonalize the covariance matrix $\boldsymbol{C}$ to obtain N nontrivial eigenvectors $\boldsymbol{v}_i$, namely, "principal mass-model vectors", which are listed in decreasing order of the eigenvalues λ_i.

Following these standard steps of PCA, one obtains the so-called PCs, represented by the principal mass-model vectors, i.e., $\boldsymbol{v}_1, \boldsymbol{v}_2, \cdots, \boldsymbol{v}_N$. Moreover, each dimension of a mass-model vector corresponds to a nucleus in the nuclear chart. The importance of a mass-model vector is represented by the corresponding eigenvalue λ_i. Thus, $\boldsymbol{v}_1$ represents the most important relevant feature extracted from these N mass models, $\boldsymbol{v}_2$ is second in importance, whereas $\boldsymbol{v}_N$ is least important. Each PC is a pattern of mass predictions for nuclei over the nuclear chart. With these PCs of nuclear mass models, one can better analyze the commonalities and differences across different mass models and build new mass models.

3 Numerical details

Six mass models, i.e., FRDM2012 [10], HFB17 [14], KTUY05 [11], D1M [15], RMF [13], and LDM [8], are selected to extract PCs. The overlap of these mass models includes 6254 nuclei; therefore, each mass-model vector, as well as each PC, is a vector in 6254-dimension Hilbert space. The mass data from AME2020 [7] are adopted to evaluate the PCs. The overlap of these mass models with the experimental data from AME2020 [7] includes 2421 nuclei, which constitute a subspace of the 6254-dimension Hilbert space. Because six mass models are considered, the components with λ_i smaller than λ_6 are irrelevant. Therefore, one obtains six

PCs extracted from these mass models, i.e., $\boldsymbol{v}_1$ for principal component-1 (PC1), $\boldsymbol{v}_2$ for PC2.

4 Results and discussion

The eigenvalues corresponding to the six PCs are presented in the second row of Table 1, together with overlaps of the six mass models (original mass-model vectors) with these six PCs (principal mass-model vectors), which are presented from the 3rd row to the 8th row. The visualizations of the six PCs are illustrated in Figures 1 and 2. Each PC is a pattern of mass predictions for nuclei over the nuclear chart. Because each PC is an eigenvector of the covariance matrix, the scale value of a PC is free. For convenience, the values presented in Figures 1 and 2 are scaled to range between −1 and 1.

Table 1 shows that among the different PCs, PC1 has the largest eigenvalue of 6.2×10^{10}; thus, it is the most important component of the mass models that contribute to the major part of nuclear masses. It is well known that the bulk properties contribute to the major part of nuclear masses. The bulk properties were originally described by the LDM model, including the volume term, surface term, Coulomb term, symmetry energy term, and odd-even term. These properties are also managed well in other mass models. Therefore, the major contributions of PC1 extracted from different mass models should correspond to the bulk properties. This correspondence is clearly depicted in Figure 1(a), where most bound nuclei are located near the iron-group elements, as described by all nuclear mass models since the LDM. The large eigenvalue of PC1 also indicates the large similarity of different mass models. This similarity is seen from the overlaps of the six mass models with PC1 (second column of Table 1), which are similar and near 0.999.

Inspection of the other PCs reveals differences with PC1. As seen in Table 1, their eigenvalues are much smaller than that of PC1, and their overlaps with different mass models are relatively small and no longer similar to each other. The eigenvalue of PC2, 3.5×10^7, is obviously larger than those of the latter PCs, which represents the second important pattern contained in the nuclear mass models. A visualization of PC2 is illustrated in Figure 1(b). One prominent feature of PC2 is the deformation properties related to the shell effects. The related magic numbers predicted by PC2 are identical to the traditional ones, as depicted in Figure 1(b) with the help of the magic lines. Another feature in Figure 1(b) is the grain structure, which is seen more clearly in the inset of Figure 1(b) as the odd-even staggering behaviors. This behavior corresponds to the odd-even effects originally from the pairing correlations and Pauli blocking. Notably, the overlap of the LDM model with PC2 is opposite to the overlaps of the other five models. This difference is due to the inclusion of the deformation effects in the other five mass models except for the LDM model.

The eigenvalues of PC3 and PC4 are small and close to each other; therefore, these two principal components are summed in Figure 2(a). The important structure of PC3+PC4 is the different behavior between the neutron- and proton-rich sides, i.e., more bound for one side and less bound for the other side. This difference might be understood as the correction of the breaking of neutron and proton symmetry energy. Several blocky structures divided by the magic lines and grain structures are also seen in Figure 2(a), indicating that some residual deformation and odd-even effects are also contained in PC3+PC4. PC5 and PC6 have even smaller eigenvalues, so they contribute less than the first four PCs. The patterns of PC5 and PC6, as shown in Figure 2(b), are much more irregular. As will be seen later, these two components only contribute an approximately 10-keV improvement to reproduce the mass data from AME2020.

Table 1 Corresponding eigenvalues of the six principal components extracted from the six mass models and the overlaps* of the six principal components with the six mass models and the experimental data from AME2020[a)]

Models	PC1	PC2	PC3	PC4	PC5	PC6
Eigenvalues	6.2×10^{10}	3.5×10^{7}	7.7×10^{6}	4.3×10^{6}	1.0×10^{6}	6.4×10^{5}
FRDM2012	0.99985	0.01275	−0.00773	−0.00267	−0.00781	−0.00087
HFB17	0.99983	0.01497	0.00038	−0.00768	0.00421	−0.00056
KTUY05	0.99986	0.01228	0.00099	−0.00890	0.00231	0.00613
D1M	0.99980	0.00023	−0.01488	0.01274	0.00291	0.00062
RMF	0.99968	0.00926	0.02160	0.00955	−0.00101	−0.00003
LDM	0.99851	−0.05428	0.00204	−0.00347	−0.00043	−0.00040
AME2020**	0.99987	0.01053	−0.00760	−0.00264	−0.00032	−0.00164

a) * The overlap of the principal component $\boldsymbol{v}_i$ with the original mass model $\boldsymbol{M}_j$ is defined as $\frac{\boldsymbol{M}_j\cdot\boldsymbol{v}_i}{\sqrt{|\boldsymbol{M}_j||\boldsymbol{v}_i|}}=\frac{\sum_k^m M_j(k)v_i(k)}{\sqrt{\sum_k^m M_j^2(k)}\sqrt{\sum_k^m v_i^2(k)}}$. ** Note that when the Hilbert space is reduced from 6254 to 2421 dimensions, the six PCs are no longer orthogonal to each other. Therefore, they are re-orthogonalized using Schmidt orthogonalization before calculating the overlaps with the data from AME2020.

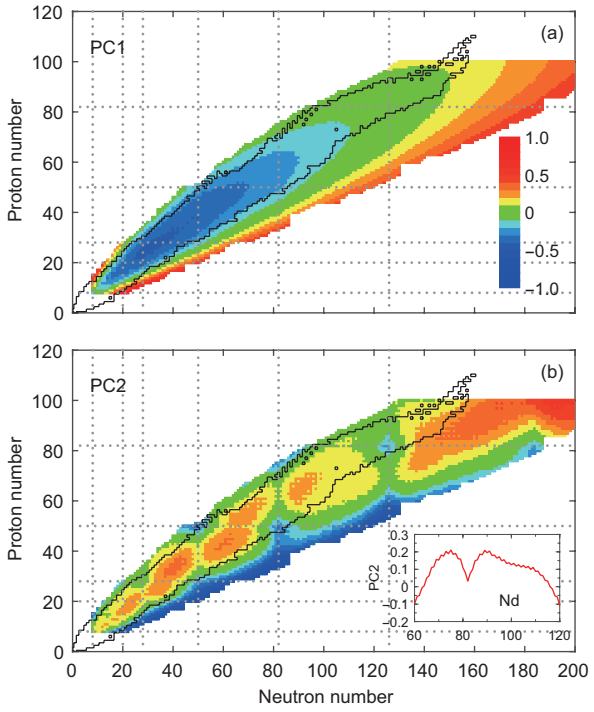

Figure 1 (Color online) Principal components, i.e., PC1 (a) and PC2 (b), of nuclear mass models with the values scaled to the range between −1 and 1. PC1 is scaled with mass number A to better illustrate the most bound nuclei around the iron-group elements. The boundary of nuclei with known masses in AME2020 is shown by the black contour lines. Dotted lines indicate the magic numbers. The inset of panel (b) presents PC2 of the Nd isotope chain.

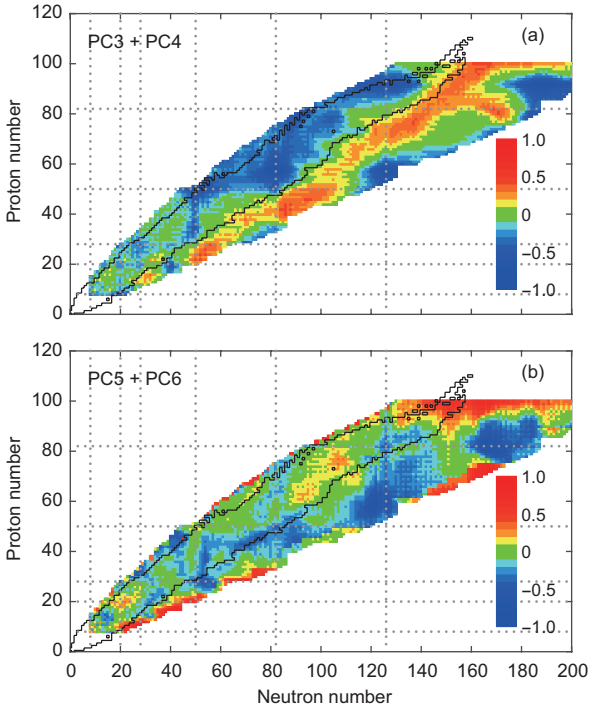

Figure 2 (Color online) Similar with Figure 1, but for PC3-PC6. PC3 and PC4 (a) are summed with the weights determined by the eigenvalues, same for PC5 and PC6 (b).

These extracted PCs of nuclear mass models can be recombined to build new mass models. The superposition coefficients are determined by the overlaps of these PCs with the mass data and are presented in Table 1. The overlaps represent the contributions of these components to reproduce the data, and they generally decrease with a decrease in the eigenvalues of these PCs. Note that the PCs and their sort orders are extracted from the theoretical mass models without any information from the experimental data from AME2020. Therefore, it is crucial to find that the order of the sizes of the contributions to reproduce the experimental data and the order of the sizes of the corresponding eigenvalues of these components are identical. Consequently, the major effects of nuclear masses have been well captured with the efforts of different mass models. New mass models can be built by including several of these PCs, i.e., from one PC to six PCs, and the corresponding superposition coefficients.

The root-mean-square (rms) deviations between new mass models, including different numbers of PCs and the experimental data from AME2020, are presented in Figure 3. As seen in Figure 3, the more PCs that are included, the higher the precision that can be achieved. The inclusion of the first PC already achieves a precision of 920 keV. The inclusions of the second, third, and fourth components work well to further improve the precision of reproducing the data. Notably, with the inclusion of the first four PCs, the new model achieves a precision of 519 keV, which is already finer than the finest precision obtained from the six original theoretical mass models, i.e., 591 keV for model HFB17. Including all six PCs reduces the rms deviation to 509 keV. Thus, by recombining the PCs extracted from the theoretical mass models, one can build a better mass model than the original theoretical models. Notably, the information or effects contained in the PCs are also contained in the six mass models.

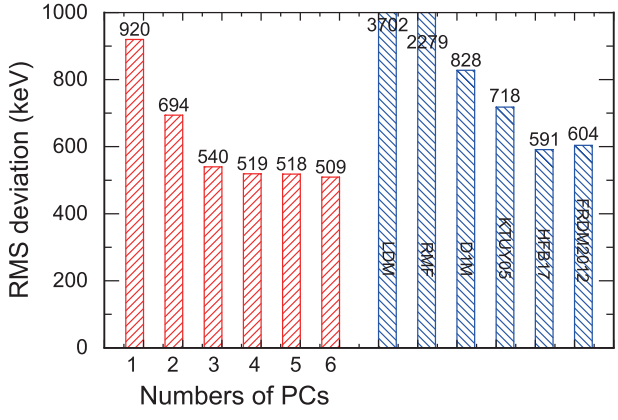

Figure 3 (Color online) Root-mean-square (rms) deviations between new mass models, including different numbers of PCs and the experimental data from AME2020. The rms deviations between the six origin mass models and the experimental data from AME2020 are also presented for comparison.

However, these effects are reintegrated by PCA technology, meaning that the effects from different mass models are reorganized to build new nuclear mass models. Therefore, the results indicate that the effects included in different theoretical mass models can collaborate to improve the prediction of nuclear masses, and this collaboration can be done using PCA technology. Note that based on the six original mass models, new mass models can be constructed by arithmetic averaging or weighted averaging (with the weights being inversely proportional to the rms deviations from the experimental data) these six models. The corresponding rms deviations obtained using these two averaging mass models are 913 and 525 keV, respectively, which are both larger than 509 keV.

To further examine this conclusion, the RCHB [16] and WS4 [9] models are added to the original six mass models, respectively, and PCA is performed for these two sets of seven mass models. The RCHB model is a nuclear mass model based on the relativistic density functional theory with continuum effects but limited to the assumption of spherical symmetry [16]. The rms deviation of the RCHB mass model from the experimental data is 7960 keV [16], larger than those of the six mass models. When the RCHB model is included, the new mass model constructed by the seven PCs has an rms deviation from the experimental mass data of 456 keV, which is obviously smaller than 509 keV. This comparison indicates that although the rms deviation of the RCHB model is large because of the spherical symmetry assumption, the effects included in the RCHB mass model can still help to improve the predictions of nuclear masses. These effects can be extracted using PCA technology. The rms deviation of the WS4 mass model from the experimental data is as small as 298 keV [9]. When the WS4 model is included, the rms deviation of the new mass model, including seven PCs, can be reduced to 292 keV, considerably smaller than 509 keV and slightly smaller than 298 keV. Thus, the effects included in the WS4 mass model can substantially help the six models to build a better mass model, and the effects in the six models can additionally help the WS4 model.

To examine the reliability of the PC-constructed mass model in predicting unknown regions, an extrapolation validation is performed. In this extrapolation validation, the superposition coefficients of the PCs are determined using experimental data with only $Z \leq 60$ nuclei being included. The new mass model constructed by the PCs with these coefficients achieves a precision of 549 keV in describing all the experimental data, which is still at the same level as 509 keV. This comparison indicates that PCA works well to avoid the overfitting problem. This capability is observed because the new mass model is constructed by the PCs extracted from theoretical mass models, and its reliability is guaranteed by the major effects included in these theoretical models. The new mass model in the experimentally unknown region thus has naturally believable reliability.

Note that the Bayesian model averaging (BMA) method [53, 70] is somewhat similar to the PCA method introduced in this work. Both methods construct new nuclear mass models in the representation space of selected nuclear mass models and aim to combine the advantages of different nuclear models. However, their differences are obvious. For the BMA method, the new mass model is constructed using weighted averaging of the selected models, where the weights are determined on the basis of Bayes' theorem. BMA has the advantage that it helps identify better models and discard poor models with the determined weights. For the PCA method, the new mass model is constructed by superpositioning the PCs of nuclear mass models. These PCs are extracted from the theoretical mass models, and they represent the major effects included in the selected mass models. The advantage of PCA is that it can extract the major effects included in the theoretical mass models and arrange them in order of importance. Therefore, one can know the most important effects contained in nuclear mass models and build a new precise mass model with only several PCs.

5 Summary

In summary, the principal component analysis approach is employed to extract the principal components contained in nuclear mass models. The effects from different nuclear mass models are reintegrated and reorganized in the extracted PCs using PCA technology. The first PC of nuclear masses is mainly contributed by the bulk property, as described in the LDM, and the second PC is mainly contributed by the deformation related to shell effects and the odd-even effects. Breaking of neutron and proton symmetry energy is also an important component that contributes to the nuclear masses and is included in the third and fourth PCs. These extracted PCs are then recombined to build new nuclear mass models. New mass models are found to achieve better accuracy in predicting the experimental mass data than the original theoretical mass models. This finding indicates that the effects contained in different theoretical models can be combined to improve the nuclear mass predictions, which can be done using PCA technology.

This study provides a new approach to building nuclear mass models by extracting the PCs of different nuclear mass models and then recombining these components. The fully *ab initio* calculations that can, in principle, include all effects, which are based on exact nuclear interactions and many-body calculations without approximation, are extremely difficult (if not impossible) to carry out for nuclear masses all over

the nuclear chart and will continue to be so even in the foreseeable future. Therefore, all nuclear mass models, including existing future models, contain some types of approximations or ignore some types of effects. In other words, they include different types and different degrees of effects on the nuclear masses. It, therefore, would be interesting to try an approach other than fully *ab initio* calculations to build nuclear mass tables that include as many effects as possible by extracting and combining the effects included in different models. This study shows that PCA technology can work as a candidate for this purpose. We also encourage theorists to develop new theoretical mass models with new effects and not be greatly concerned about the balance of including new effects and accurately reproducing experimental data because PCA technology can extract the new effects and make them contribute to improving nuclear mass predictions.

This work was supported by the State Key Laboratory of Nuclear Physics and Technology, Peking University (Grant No. NPT2023KFY02), the China Postdoctoral Science Foundation (Grant No. 2021M700256), the National Key R&D Program of China (Grant No. 2018YFA0404400), the National Natural Science Foundation of China (Grant Nos. 11935003, 11975031, 12141501, and 12070131001), and the High-performance Computing Platform of Peking University.

Conflict of interest The authors declare that they have no conflict of interest.

1 D. Lunney, J. M. Pearson, and C. Thibault, Rev. Mod. Phys. **75**, 1021 (2003).
2 M. R. Mumpower, R. Surman, G. C. McLaughlin, and A. Aprahamian, Prog. Particle Nucl. Phys. **86**, 86 (2016), arXiv: 1508.07352.
3 Z. Li, Z. M. Niu, and B. H. Sun, Sci. China-Phys. Mech. Astron. **62**, 982011 (2019).
4 X. F. Jiang, X. H. Wu, and P. W. Zhao, Astrophys. J. **915**, 29 (2021), arXiv: 2105.10218.
5 X. H. Wu, P. W. Zhao, S. Q. Zhang, and J. Meng, Astrophys. J. **941**, 152 (2022), arXiv: 2108.06104.
6 J. Meng, Z. M. Niu, H. Z. Liang, and B. H. Sun, Sci. China-Phys. Mech. Astron. **54**, 119 (2011).
7 M. Wang, W. J. Huang, F. G. Kondev, G. Audi, and S. Naimi, Chin. Phys. C **45**, 030003 (2020).
8 C. F. Weizsäcker, Z. Physik **96**, 431 (1935).
9 N. Wang, M. Liu, X. Wu, and J. Meng, Phys. Lett. B **734**, 215 (2014), arXiv: 1405.2616.
10 P. Möller, A. J. Sierk, T. Ichikawa, and H. Sagawa, Atom. Data Nucl. Data Tables **109-110**, 1 (2016).
11 H. Koura, T. Tachibana, M. Uno, and M. Yamada, Prog. Theor. Phys. **113**, 305 (2005).
12 J. M. Pearson, R. C. Nayak, and S. Goriely, Phys. Lett. B **387**, 455 (1996).
13 L. Geng, H. Toki, and J. Meng, Prog. Theor. Phys. **113**, 785 (2005), arXiv: nucl-th/0503086.
14 S. Goriely, N. Chamel, and J. M. Pearson, Phys. Rev. Lett. **102**, 152503 (2009), arXiv: 0906.2607.
15 S. Goriely, S. Hilaire, M. Girod, and S. Péru, Phys. Rev. Lett. **102**, 242501 (2009).
16 X. W. Xia, Y. Lim, P. W. Zhao, H. Z. Liang, X. Y. Qu, Y. Chen, H. Liu, L. F. Zhang, S. Q. Zhang, Y. Kim, and J. Meng, Atom. Data Nucl. Data Tables **121-122**, 1 (2018), arXiv: 1704.08906.
17 X. Meng, B. N. Lu, and S. G. Zhou, Sci. China-Phys. Mech. Astron. **63**, 212011 (2020), arXiv: 1910.10552.
18 J. Erler, N. Birge, M. Kortelainen, W. Nazarewicz, E. Olsen, A. M. Perhac, and M. Stoitsov, Nature **486**, 509 (2012).
19 A. V. Afanasjev, S. E. Agbemava, D. Ray, and P. Ring, Phys. Lett. B **726**, 680 (2013), arXiv: 1309.3289.
20 Y. L. Yang, Y. K. Wang, P. W. Zhao, and Z. P. Li, Phys. Rev. C **104**, 054312 (2021), arXiv: 2108.13057.
21 K. Zhang, M. K. Cheoun, Y. B. Choi, P. S. Chong, J. Dong, Z. Dong, X. Du, L. Geng, E. Ha, X. T. He, C. Heo, M. C. Ho, E. J. In, S. Kim, Y. Kim, C. H. Lee, J. Lee, H. Li, Z. Li, T. Luo, J. Meng, M. H. Mun, Z. Niu, C. Pan, P. Papakonstantinou, X. Shang, C. Shen, G. Shen, W. Sun, X. X. Sun, C. K. Tam, C. K. Thaivayongnou, C. Wang, X. Wang, S. H. Wong, J. Wu, X. Wu, X. Xia, Y. Yan, R. W. Y. Yeung, T. C. Yiu, S. Zhang, W. Zhang, X. Zhang, Q. Zhao, and S. G. Zhou, Atom. Data Nucl. Data Tables **144**, 101488 (2022).
22 C. Pan, M. K. Cheoun, Y. B. Choi, J. Dong, X. Du, X. H. Fan, W. Gao, L. Geng, E. Ha, X. T. He, J. Huang, K. Huang, S. Kim, Y. Kim, C. H. Lee, J. Lee, Z. Li, Z. R. Liu, Y. Ma, J. Meng, M. H. Mun, Z. Niu, P. Papakonstantinou, X. Shang, C. Shen, G. Shen, W. Sun, X. X. Sun, J. Wu, X. Wu, X. Xia, Y. Yan, T. C. Yiu, K. Zhang, S. Zhang, W. Zhang, X. Zhang, Q. Zhao, R. Zheng, and S. G. Zhou, Phys. Rev. C **106**, 014316 (2022), arXiv: 2205.01329.
23 B. H. Sun, P. W. Zhao, and J. Meng, Sci. China-Phys. Mech. Astron. **54**, 210 (2011).
24 X. M. Hua, T. H. Heng, Z. M. Niu, B. H. Sun, and J. Y. Guo, Sci. China-Phys. Mech. Astron. **55**, 2414 (2012).
25 X. Y. Qu, Y. Chen, S. Q. Zhang, P. W. Zhao, I. J. Shin, Y. Lim, Y. Kim, and J. Meng, Sci. China-Phys. Mech. Astron. **56**, 2031 (2013), arXiv: 1309.3987.
26 J. Barea, A. Frank, J. G. Hirsch, P. V. Isacker, S. Pittel, and V. Velázquez, Phys. Rev. C **77**, 041304 (2008).
27 M. Bao, Z. He, Y. Y. Cheng, Y. M. Zhao, and A. Arima, Sci. China-Phys. Mech. Astron. **60**, 022011 (2017).
28 W. E. Ormand, Phys. Rev. C **55**, 2407 (1997), arXiv: nucl-th/9701002.
29 G. J. Fu, Y. Lei, H. Jiang, Y. M. Zhao, B. Sun, and A. Arima, Phys. Rev. C **84**, 034311 (2011).
30 G. Carleo, I. Cirac, K. Cranmer, L. Daudet, M. Schuld, N. Tishby, L. Vogt-Maranto, and L. Zdeborová, Rev. Mod. Phys. **91**, 045002 (2019), arXiv: 1903.10563.
31 A. Boehnlein, M. Diefenthaler, N. Sato, M. Schram, V. Ziegler, C. Fanelli, M. Hjorth-Jensen, T. Horn, M. P. Kuchera, D. Lee, W. Nazarewicz, P. Ostroumov, K. Orginos, A. Poon, X. N. Wang, A. Scheinker, M. S. Smith, and L. G. Pang, Rev. Mod. Phys. **94**, 031003 (2022), arXiv: 2112.02309.
32 W. He, Q. Li, Y. Ma, Z. Niu, J. Pei, and Y. Zhang, Sci. China-Phys. Mech. Astron. **66**, 282001 (2023), arXiv: 2301.06396.
33 W. B. He, Y. G. Ma, L. G. Pang, H. C. Song, and K. Zhou, Nucl. Sci. Tech. **34**, 88 (2023).
34 Y. G. Ma, L. G. Pang, R. Wang, and K. Zhou, Chin. Phys. Lett. **40**, 122101 (2023), arXiv: 2311.07274.
35 Y. Wang, and Q. Li, Front. Phys. **18**, 64402 (2023), arXiv: 2305.16686.
36 E. Alhassan, D. Rochman, A. Vasiliev, M. Hursin, A. J. Koning, and H. Ferroukhi, Nucl. Sci. Tech. **33**, 50 (2022).
37 K. Zhou, L. Wang, L. G. Pang, and S. Shi, Prog. Particle Nucl. Phys. **135**, 104084 (2024).
38 X. H. Wu, and P. W. Zhao, Phys. Rev. C **101**, 051301 (2020).
39 X. H. Wu, L. H. Guo, and P. W. Zhao, Phys. Lett. B **819**, 136387 (2021), arXiv: 2105.10634.
40 X. H. Wu, Y. Y. Lu, and P. W. Zhao, Phys. Lett. B **834**, 137394 (2022), arXiv: 2208.13966.
41 L. Guo, X. Wu, and P. Zhao, Symmetry **14**, 1078 (2022).
42 X. K. Du, P. Guo, X. H. Wu, and S. Q. Zhang, Chin. Phys. C **47**, 074108 (2023).
43 X. H. Wu, Front. Phys. **11**, 1061042 (2023).
44 N. Wang, and M. Liu, Phys. Rev. C **84**, 051303 (2011), arXiv:

1111.0354.
45 Z. M. Niu, Z. L. Zhu, Y. F. Niu, B. H. Sun, T. H. Heng, and J. Y. Guo, Phys. Rev. C **88**, 024325 (2013), arXiv: 1309.0407.
46 N. N. Ma, H. F. Zhang, P. Yin, X. J. Bao, and H. F. Zhang, Phys. Rev. C **96**, 024302 (2017).
47 Z. Niu, H. Liang, B. Sun, Y. Niu, J. Guo, and J. Meng, Sci. Bull. **63**, 759 (2018), arXiv: 1807.05535.
48 R. Utama, J. Piekarewicz, and H. B. Prosper, Phys. Rev. C **93**, 014311 (2016), arXiv: 1508.06263.
49 Z. M. Niu, and H. Z. Liang, Phys. Lett. B **778**, 48 (2018), arXiv: 1801.04411.
50 L. Neufcourt, Y. Cao, W. Nazarewicz, and F. Viens, Phys. Rev. C **98**, 034318 (2018), arXiv: 1806.00552.
51 Z. M. Niu, and H. Z. Liang, Phys. Rev. C **106**, L021303 (2022), arXiv: 2208.04783.
52 X. C. Ming, H. F. Zhang, R. R. Xu, X. D. Sun, Y. Tian, and Z. G. Ge, Nucl. Sci. Tech. **33**, 48 (2022).
53 L. Neufcourt, Y. Cao, W. Nazarewicz, E. Olsen, and F. Viens, Phys. Rev. Lett. **122**, 062502 (2019), arXiv: 1901.07632.
54 M. Shelley, and A. Pastore, Universe **7**, 131 (2021), arXiv: 2102.07497.
55 H. F. Zhang, L. H. Wang, J. P. Yin, P. H. Chen, and H. F. Zhang, J. Phys. G-Nucl. Part. Phys. **44**, 045110 (2017).
56 Z. P. Gao, Y. J. Wang, H. L. Lü, Q. F. Li, C. W. Shen, and L. Liu, Nucl. Sci. Tech. **32**, 109 (2021).
57 Y. Liu, C. Su, J. Liu, P. Danielewicz, C. Xu, and Z. Ren, Phys. Rev. C **104**, 014315 (2021).
58 A. Idini, Phys. Rev. Res. **2**, 043363 (2020), arXiv: 1904.00057.
59 S. Wold, K. Esbensen, and P. Geladi, Chemometr. Intell. Lab. Syst. **2**, 37 (1987).
60 I. T. Jolliffe, *Principal Component Analysis for Special Types of Data* (Springer, New York, 2002).
61 C. Augier, A. S. Barabash, F. Bellini, G. Benato, M. Beretta, L. Bergé, J. Billard, Y. A. Borovlev, L. Cardani, N. Casali, A. Cazes, E. Celi, M. Chapellier, D. Chiesa, I. Dafinei, F. A. Danevich, M. De Jesus, T. Dixon, L. Dumoulin, K. Eitel, F. Ferri, B. K. Fujikawa, J. Gascon, L. Gironi, A. Giuliani, V. D. Grigorieva, M. Gros, D. L. Helis, H. Z. Huang, R. Huang, L. Imbert, J. Johnston, A. Juillard, H. Khalife, M. Kleifges, V. V. Kobychev, Y. G. Kolomensky, S. I. Konovalov, J. Kotila, P. Loaiza, L. Ma, E. P. Makarov, P. de Marcillac, R. Mariam, L. Marini, S. Marnieros, X. F. Navick, C. Nones, E. B. Norman, E. Olivieri, J. L. Ouellet, L. Pagnanini, L. Pattavina, B. Paul, M. Pavan, H. Peng, G. Pessina, S. Pirro, D. V. Poda, O. G. Polischuk, S. Pozzi, E. Previtali, T. Redon, A. Rojas, S. Rozov, V. Sanglard, J. A. Scarpaci, B. Schmidt, Y. Shen, V. N. Shlegel, F. Šimkovic, V. Singh, C. Tomei, V. I. Tretyak, V. I. Umatov, L. Vagneron, M. Velázquez, B. Ware, B. Welliver, L. Winslow, M. Xue, E. Yakushev, M. Zarytskyy, and A. S. Zolotarova, Phys. Rev. Lett. **131**, 162501 (2023), arXiv: 2307.14086.
62 D. Akimov, P. An, C. Awe, P. S. Barbeau, B. Becker, V. Belov, I. Bernardi, M. A. Blackston, C. Bock, A. Bolozdynya, J. Browning, B. Cabrera-Palmer, D. Chernyak, E. Conley, J. Daughhetee, J. Detwiler, K. Ding, M. R. Durand, Y. Efremenko, S. R. Elliott, L. Fabris, M. Febbraro, A. Gallo Rosso, A. Galindo-Uribarri, M. P. Green, M. R. Heath, S. Hedges, D. Hoang, M. Hughes, T. Johnson, A. Khromov, A. Konovalov, E. Kozlova, A. Kumpan, L. Li, J. M. Link, J. Liu, K. Mann, D. M. Markoff, J. Mastroberti, P. E. Mueller, J. Newby, D. S. Parno, S. I. Penttila, D. Pershey, R. Rapp, H. Ray, J. Raybern, O. Razuvaeva, D. Reyna, G. C. Rich, J. Ross, D. Rudik, J. Runge, D. J. Salvat, A. M. Salyapongse, K. Scholberg, A. Shakirov, G. Simakov, G. Sinev, W. M. Snow, V. Sosnovstsev, B. Suh, R. Tayloe, K. Tellez-Giron-Flores, I. Tolstukhin, E. Ujah, J. Vanderwerp, R. L. Varner, C. J. Virtue, G. Visser, T. Wongjirad, Y. R. Yen, J. Yoo, C. H. Yu, and J. Zettlemoyer, Phys. Rev. Lett. **129**, 081801 (2022), arXiv: 2110.07730.
63 R. S. Bhalerao, J. Y. Ollitrault, S. Pal, and D. Teaney, Phys. Rev. Lett. **114**, 152301 (2015), arXiv: 1410.7739.
64 E. Bonilla, P. Giuliani, K. Godbey, and D. Lee, Phys. Rev. C **106**, 054322 (2022), arXiv: 2203.05284.
65 X. H. Wu, Z. X. Ren, and P. W. Zhao, Phys. Rev. C **105**, L031303 (2022), arXiv: 2105.07696.
66 A. Bulgac, M. M. N. Forbes, S. Jin, R. N. Perez, and N. Schunck, Phys. Rev. C **97**, 044313 (2018), arXiv: 1708.08771.
67 J. M. R. Fox, C. W. Johnson, and R. N. Perez, Phys. Rev. C **101**, 054308 (2020), arXiv: 1911.05208.
68 V. Kejzlar, L. Neufcourt, W. Nazarewicz, and P. G. Reinhard, J. Phys. G-Nucl. Part. Phys. **47**, 094001 (2020), arXiv: 2002.04151.
69 N. Schunck, J. O'Neal, M. Grosskopf, E. Lawrence, and S. M. Wild, J. Phys. G-Nucl. Part. Phys. **47**, 074001 (2020), arXiv: 2003.12207.
70 X. Y. Zhang, W. F. Li, J. Y. Fang, and Z. M. Niu, Nucl. Phys. A **1043**, 122820 (2024).